BIOCHEMISTRY
including biophysical chemistry & molecular biology

Article

pubs.acs.org/biochemistry

Cross-Linking Mass Spectrometry and Mutagenesis Confirm the Functional Importance of Surface Interactions between CYP3A4 and Holo/Apo Cytochrome b_5

Chunsheng Zhao,[†] Qiuxia Gao,[†] Arthur G. Roberts,[§] Scott A. Shaffer,[‡] Catalin E. Doneanu,[†] Song Xue,[∥] David R. Goodlett,[†] Sidney D. Nelson,[†] and William M. Atkins*[,†]

[†]Department of Medicinal Chemistry, University of Washington, Box 357610, Seattle, Washington 98195, United States

[‡]Biochemistry and Molecular Pharmacology, University of Massachusetts Medical School, Shrewsbury, Massachusetts 01545, United States

[§]Pharmaceutical and Biomedical Sciences, University of Georgia, Athens, Georgia 30605, United States

[∥]Microsoft Inc., 1 Microsoft Way, Redmond, Washington 98052, United States

Supporting Information

ABSTRACT: Cytochrome b_5 (cyt b_5) is one of the key components in the microsomal cytochrome P450 monooxygenase system. Consensus has not been reached about the underlying mechanism of cyt b_5 modulation of CYP catalysis. Both cyt b_5 and apo b_5 are reported to stimulate the activity of several P450 isoforms. In this study, the surface interactions of both holo and apo b_5 with CYP3A4 were investigated and compared for the first time. Chemical cross-linking coupled with mass spectrometric analysis was used to identify the potential electrostatic interactions between the protein surfaces. Subsequently, the models of interaction of holo/apo b_5 with CYP3A4 were built using the identified interacting sites as constraints. Both cyt b_5 and apo b_5 were predicted to bind to the same groove on CYP3A4 with close contacts to the B−B′ loop of CYP3A4, a substrate recognition site. Mutagenesis studies further confirmed that the interacting sites on CYP3A4 (Lys96, Lys127, and Lys421) are functionally important. Mutation of these residues reduced or abolished cyt b_5 binding affinity. The critical role of Arg446 on CYP3A4 in binding to cyt b_5 and/or cytochrome P450 reductase was also discovered. The results indicated that electrostatic interactions on the interface of the two proteins are functionally important. The results indicate that apo b_5 can dock with CYP3A4 in a manner analogous to that of holo b_5, so electron transfer from cyt b_5 is not required for its effects.

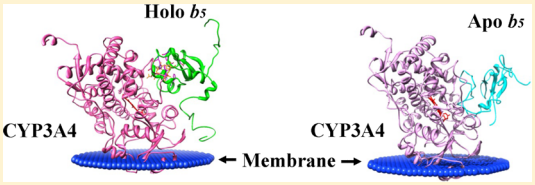

Microsomal cytochrome P450s (CYPs) catalyze biotransformation of a wide variety of chemically and structurally diverse compounds. These reactions account for approximately 85−90% of therapeutic drug metabolism.[1] Each reaction cycle of microsomal CYPs requires sequential input of two electrons, which activates a molecule of oxygen to complete the reaction.[1] In microsomal systems, electrons are transferred from NADPH, through CPR and/or cyt b_5, to CYPs. CPR is an indispensable component of the catalytic cycle because the initial reduction of CYP (the introduction of the first electron) is catalyzed predominantly by CPR.[1] In contrast, the mechanism of the second electron transfer and the role of cyt b_5 in the P450 catalytic cycle are not completely understood.

Cyt b_5 exhibits complex effects on CYP-catalyzed reactions. The effects are dependent on both CYP isoform and substrate. It can stimulate, inhibit, or have no effect on CYP-catalyzed reactions. Cyt b_5 may act as an obligate component, or a modifier, of a reaction. It has been reported that the activity of more than 20 CYP isoforms can be modulated by cyt b_5, including the majority of the human drug-metabolizing CYPs.[2,3] For example, cyt b_5 is absolutely required for the metabolism of methoxyflurane, prostaglandins A1, E1, and E2 by CYP2B4,[4] 7-ethoxycoumarin, chlorzoxazone, aniline, and *N*-nitrosodimethylamine by CYP2E1,[5] *p*-nitrophenetole O-deethylation by CYP2B1,[6] and arachidonate by CYP4A7.[7] On the other hand, some CYPs show higher activity in the presence of cyt b_5 than in the absence of cyt b_5, such as CYP2A6-catalyzed coumarin 7-hydroxylation, CYP3A4-catalyzed testosterone (TST) 6β-hydroxylation, CYP2C19-catalyzed *S*-mephenytoin 4′-hydroxylation,[8,9] etc. Reactions inhibited by cyt b_5 include CYP2B4-catalyzed benzphetamine demethylation.[10] In contrast, cyt b_5 shows no effect on CYP1A2- and CYP2D6-catalyzed reactions,[8] or benzo[*a*]pyrene hydroxylation by CYP2B4.[11]

Cyt b_5 affects CYPs by several possible mechanisms.[3] One asserts that cyt b_5 facilitates a fast second electron transfer, which is putatively the rate-limiting step in the CYP catalytic cycle and therefore stimulates some CYP activities such as in CYP2E1 and rabbit CYP2B4.[3,12,13] Cyt b_5 has also been suggested to decrease the level of uncoupling of the

Received: August 8, 2012
Revised: October 29, 2012
Published: November 14, 2012

dx.doi.org/10.1021/bi301069r | *Biochemistry* 2012, 51, 9488−9500

monooxygenase reaction through its interaction with CYPs and to result in an increased catalytic efficiency. A third proposed mechanism suggests that a heterodimeric CYP−cyt b_5 complex[3] is formed, which is able to accept two electrons from CPR to form a two-electron-reduced complex species.[14] This complex facilitates formation of the active peroxo P450 species as it excludes the need of two interactions with CPR. An additional suggested mechanism is the allosteric effect, in which cyt b_5 leads to conformational changes of CYPs, resulting in a modulated catalytic efficiency. This mechanism continues to be supported by recent data,[8,9,15] but its importance is unclear.[5,10,16] Among these mechanisms, the two basic roles of cyt b_5 are proposed to be electron transfer and an allosteric effect via a conformational change induced by cyt b_5 on CYP. There is no consensus about whether the transfer of an electron from cyt b_5 is required or whether allosteric effects of cyt b_5 are involved. Because the effects of cyt b_5 on CYPs require complex formation,[17] identification of protein interacting regions and protein orientation in the redox complexes can be important for understanding the mechanisms and effects of cyt b_5.[18]

We have previously defined the structural interaction between CYP2E1 and cyt b_5.[19] In the CYP2E1−cyt b_5 complex model, the cyt b_5 heme group protrudes toward the surface of CYP2E1, to which the buried heme of CYP2E1 is closest.[19] CYP2E1 is a CYP isoform whose reactions are highly stimulated by cyt b_5,[2,9,20] but not by apo b_5 (cyt b_5 devoid of heme).[9,20] The requirement of the cyt b_5 heme group for the CYP2E1-catalyzed reaction supports the mechanism of facilitating electron transfer rather than only causing an allosteric effect for this particular isoform. Intermolecular electrostatic interactions are the main stabilizing forces for CYP−cyt b_5 interactions[3] and contribute to the proper orientations of the heme prosthetic groups. Overall, this intermolecular electrostatic interaction can result in a change in the dielectric constant and the subsequent facilitation of the electron transfer process.[21]

Unlike its effects on CYP2E1 reactions, cyt b_5 mainly exerts an allosteric effect on CYP3A4 reactions as suggested by previous studies.[22,23] Apo b_5 has also been shown to stimulate some of CYP3A4-catalyzed reactions, such as testosterone 6β-hydroxylation and nifedipine oxidation, to a slightly lesser extent than holo b_5 (natural cyt b_5).[24] Nuclear magnetic resonance (NMR) studies have confirmed that removal of the heme group from cyt b_5 has an only minimal influence on its secondary structure.[25−27] The structural effects of heme removal are highly localized, so the stimulatory effect of apo b_5 on CYP3A4 indicates an allosteric mechanism. In addition, cyt b_5 changes the product regioselectivity and turnover kinetics of some CYP3A4 reactions, such as triazolam and pyrene oxidation,[28,29] suggesting topological changes in the active site of CYP3A4.[30] These observations provide additional evidence of an allosteric mechanism of cyt b_5 on CYP3A4.

Extending these studies to the surface interactions between cyt b_5 and CYP3A4 can further elucidate the complicated mechanism of cyt b_5 in the stimulation of CYPs. Chemical cross-linking and mass spectrometry were used to structurally characterize the sites of interaction between cyt b_5 and CYP3A4 because of the advantage of requiring small amounts of sample and the high degree of accuracy in determining the structures; site-directed mutagenesis and metabolic activity assays were used to confirm the functional importance of the identified interacting sites. The identified cyt b_5−CYP3A4 interacting sites allowed construction of models for the holo/apo b_5−CYP3A4 interactions by computational calculation. The results of this study indicate that an allosteric effect of cyt b_5 contributes to the modulation of CYP3A4 reactions.

EXPERIMENTAL PROCEDURES

Materials. Plasmid $(His)_4$HMWHuman-cyt b_5 was kindly provided by R. J. Auchus (University of Michigan, Ann Arbor, MI).[31,32] Restriction enzymes and other DNA-modifying enzymes were from New England BioLabs (Beverly, MA). Platinum *Pfx* DNA polymerase, T4 DNA ligase, histidine-tagged recombinant human cyt b_5, and Vivid 3A4 substrate DBOMF were from Invitrogen (Carlsbad, CA). The QuikChange site-directed mutagenesis kit was from Stratagene (La Jolla, CA). Bactotryptone, bactopeptone, and bactoyeast extract were from BD Biosciences Clontech (Palo Alto, CA). Emulgen 911 was from Kao Chemicals (Tokyo, Japan). IPTG (isopropyl β-D-1-thiogalactopyranoside), δ-ALA (5-aminolevulinic acid), thiamine, imidazole hydrochloride, protease inhibitor cocktail, sodium cholate, and dithiothreitol were from Sigma-Aldrich (St. Louis, MO). The CHT ceramic hydroxyapatite column (type I, 40 μm particle size) was from Bio-Rad (Hercules, CA). L-α-Dilauroyl-*sn*-glycero-3-phosphocholine (DLPC), L-α-dioleoyl-*sn*-glycero-3-phosphocholine (DOPC), and L-α-dilauroyl-*sn*-glycero-3-phosphoserine (DLPS) were from Avanti Polar Lipids, Inc. (Alabaster, AL). Ni-NTA Superflow was from Qiagen (Valencia, CA). The cross-linking reagent 1-ethyl-3-[3-(dimethylamino)propyl]-carbodiimide hydrochloride (EDC) was from Pierce Biotechnology, Inc. (Rockford, IL). Sequencing grade modified trypsin was from Roche Applied Science (Indianapolis, IN). ^{18}O-labeled water (99 atom % ^{18}O) was from Isotec (Miamisburg, OH). HPLC solvents were of HPLC grade. All other reagents were of analytical grade.

Site-Directed Mutagenesis of CYP3A4. For site-directed mutagenesis of CYP3A4, the oligonucleotide primers used in the generation of CYP3A4 mutations K96A, K127A, K421A, and R446A were as follows (mismatches indicated by the underlined bases): K96A forward, 5′ CAA AAC AGT GCT AGT GGC AGA ATG TTA TTC TGT CTT C 3′; K96A reverse, 5′ GAA GAC AGA ATA ACA TTC TGC CAC TAG CAC TGT TTT G 3′; K127A forward, 5′ GCT GAG GAT GAA GAA TGG GCG AGA TTA CGA TCA TTG C 3′; K127A reverse, 5′ GCA ATG ATC GTA ATC TCG CCC ATT CTT CAT CCT CAG C 3′; K421A forward, 5′ CTC CCT GAA AGA TTC AGC GCG AAG AAC AAG GAC AAC 3′; K421A reverse, 5′ GTT GTC CTT GTT CTT CGC GCT GAA TCT TTC AGG GAG 3′; R446A forward, 5′ CCA GAA ACT GCA TTG GCA TGG CGT TTG CTC TCA TG 3′; R446A reverse, 5′ CAT GAG AGC AAA CGC CAT GCC AAT GCA GTT TCT GG 3′. For the construction of a CYP3A4 triple mutant (K96A/K127A/K421A), a CYP3A4 K96A/K421A double mutation was first constructed using the K421A single mutation plasmid as the template and the K96A forward and reverse primers; afterward, the K96A/K127A/K421A triple mutation was constructed using the K96A/K421A plasmid as the template and the K127A forward and reverse primers. The mutagenesis was performed using the QuikChange site-directed mutagenesis kit according to the manufacturer's protocol. The full-length cDNAs of the CYP3A4 sequence containing the desired mutations were analyzed at the University of Washington Sequencing Facility.

Protein Expression and Purification. N-Terminally truncated CYP3A4 and mutations were produced in *Escherichia*

coli C41 cells using expression vector pCWhum3A4 $(His)_6$. Growth and induction of *E. coli* C41 cells were performed as described previously.[33] Solubilized membranes were prepared, and CYP3A4 was purified on the Ni-NTA agarose column as described in ref 34. The column was equilibrated and loaded with equilibration buffer [50 mM KP_i (pH 7.4), 20% glycerol, 0.05% sodium cholate, 5 mM imidazole, and 50 μM testosterone] and then washed with 20 column volumes of wash buffer [50 mM KP_i (pH 7.4), 20% glycerol, 0.05% sodium cholate, 40 mM imidazole, 100 mM glycine, 0.3 M sodium chloride, 0.2% Emulgen 911, 20 mM β-mercaptoethanol, and 50 μM testosterone]. The protein was eluted with a minimal volume of elution buffer [50 mM KP_i (pH 7.4), 20% glycerol, 350 mM imidazole, and 0.02% sodium cholate] and then dialyzed against hydroxyapatite (HA) equilibration buffer (10 mM KP_i, 2 mM BME, 0.2% cholate, and 20% glycerol). The protein was then loaded onto the HA column, washed with HA wash buffer [25 mM KP_i, 2 mM BME, and 20% glycerol (pH 7.4)], eluted with 400 mM KP_i and 20% glycerol (pH 7.4), and dialyzed into storage buffer [100 mM KP_i (pH 7.4), 20% glycerol, 0.5 mM EDTA, and 0.1 mM DTT]. The CYP3A4 content was determined by reduced carbon monoxide difference spectra.[34]

Apo b_5 was prepared from human cyt b_5 according to a previously published protocol.[5,35,36] The expression and purification of human cyt b_5 were conducted according to previously described protocols.[32,36] The reconstituted holo b_5 activity was comparable with that of commercial cyt b_5 from Invitrogen (data not shown) and was used for the equilibrium binding assay. In all other holo b_5 assays, commercial holo b_5 was used. The expression and purification of rat CPR were performed as previously described.[37,38]

Cross-Linking Reactions. Electrostatic interactions are considered to be the major driving force in cyt b_5−CYP3A4 interactions.[39−41] Therefore, EDC, a water-soluble cross-linking reagent, was chosen to "trap" the interaction between cyt b_5 and CYP3A4, as EDC can cross-link basic (Lys) and acidic (Asp or Glu) residues that come very close to each other.[42] It generates amide bonds, with a "zero-length" linker between the bonded species. The zero-length linker limits the number of orientations that must be considered in building structural models based on cross-linking data. CYP3A4 and cyt b_5 were reconstituted at a molar ratio of 1:1 in 100 μL of 50 mM KP_i buffer in the presence of liposomes[15,43] [1:1:1 (w/w/w) DLPC/DOPC/DLPS lipid mixture, with final concentrations of 10 μM for each enzyme]. The solution was gently stirred for 10 min and held at room temperature for 2 h. Then the chemical cross-linking reagent EDC was added to a final concentration of 10 mM from a 100 mM stock. The reaction was allowed to proceed at room temperature for 2 h followed by dialysis against 50 mM KP_i buffer and 50 mM ammonium bicarbonate buffer to remove EDC and isourea that was generated.

Proteolytic Digestion and Mass Spectrometric Analysis. Digestion of the cross-linked protein complex was performed as previously described.[19] Subsequent mass spectrometric analysis for holo b_5 and CYP3A4 cross-linking was conducted as described previously[44] using ^{18}O labeling. Mass spectrometric analysis of apo b_5 and CYP3A4 cross-linking was assessed using a recently published method,[45] which has the advantage of not requiring stable isotopic labeling. An LTQ-Orbitrap (ThermoFisher, San Jose, CA) was used to acquire all MS data at high mass accuracy (typically 0.1−3.0 ppm) because this limits false positives from the large number of possible cross-linked peptide candidates. Cross-linked peptides analyzed by ESI tend to have twice the charge of their linear constituents. This allows the data-dependent ion selection process for collision-induced dissociation (CID) to be focused only on precursors with a charge state of ≥3, thus focusing data acquisition on the peptide more likely to be cross-linked. The data were analyzed with the open-modification algorithm Popitam.[45] Tandem mass spectra were further analyzed and sequence matches confirmed and assigned with the MS3D collaboratory portal[46,47] and University of Washington Proteomics Center web tools as references.

Testosterone 6β-Hydroxylation and Fluorogenic Vivid 3A4 Substrate Metabolism Catalyzed by Wild-Type CYP3A4 and Its Mutants. Working buffers for CYP3A4 incubations were prepared following a published protocol.[48] Basically, the final reaction buffer contains 0.2 μM CYP3A4, 0.4 μM NADPH-dependent cytochrome P450 reductase (CPR), 0.2 μM cyt b_5, 0.1 mg/mL CHAPS, a 0.02 mg/mL lipid mixture, 3 mM GSH, and 30 mM $MgCl_2$ in 50 mM potassium HEPES buffer (pH 7.4). The testosterone 6β-hydroxylation assay was conducted according to a previously described procedure[48] except that 1 μg of 11α-hydroxyprogesterone per reaction was used as an internal standard. The Vivid Green assay was conducted according to the supplier's protocol. Both assays were conducted at a fixed CYP3A4:CPR:cyt b_5 enzyme ratio of 1:2:1 unless otherwise noted.

Equilibrium Binding. For the cyt b_5−CYP3A4 affinity assay, experiments were conducted using the method described earlier with slightly modified buffer conditions.[16,49] Briefly, the sample cuvette contained 0.2 μM CYP3A4 in reaction buffer (pH 7.4) as used for activity assays. The reference cuvette contained only reaction buffer (pH 7.4). The difference spectra of the two cuvettes were recorded. Next, cyt b_5 (0−3 μM) was titrated into both sample and reference cuvettes, and both were scanned from 340 to 500 nm to monitor the peak heights of the low-spin (418 nm) and high-spin (390 nm) Soret bands. The changes in the difference between the two peaks in the absolute spectra were plotted versus cyt b_5 concentration to estimate the binding affinity of cyt b_5 for CYP3A4. The dissociation constant (K_d) was determined using the following equation as described in ref 50

$$\Delta A = \Delta A_{max}\{(K_d + [\text{CYP3A4}] + [b_5])/2 - [(K_d + [\text{CYP3A4}] + [b_5])^2/4 - [\text{CYP3A4}][b_5]]^{1/2}\} \quad (1)$$

where ΔA is the change in absorbance difference between 390 and 418 nm, ΔA_{max} is the maximal absorbance change, [CYP3A4] is 200 nM in the assay, $[b_5]$ is the concentration of holo b_5 or apo b_5, and K_d is the spectral dissociation constant of the CYP3A4−b_5 complex.

For the TST binding affinity assay, 1 μM CYP3A4 was used in a buffer that consisted of 50 mM KP_i and 20% glycerol. The change in absorbance difference between 390 and 418 nm (ΔA) was plotted as a function of TST concentration.[51,52] Apparent dissociation constants were estimated using the Hill equation (eq 2) with GraphPad:

$$\Delta A = A_{max} \times S^n/[K_{d(app)} + S^n] \quad (2)$$

where A_{max} is the maximal absorbance change, S is the TST concentration, $K_{d(app)}$ is the apparent dissociation constant (the

dx.doi.org/10.1021/bi301069r | *Biochemistry* 2012, 51, 9488−9500

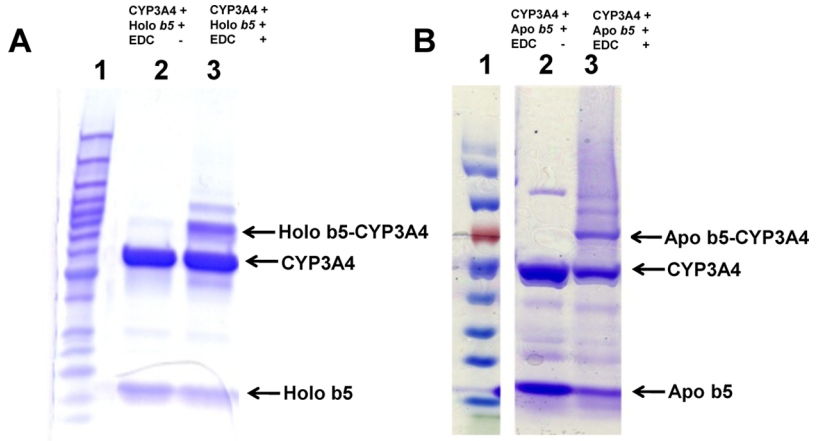

Figure 1. Sodium dodecyl sulfate–polyacrylamide gel electrophoresis analysis of the cross-linking reactions of human cyt b_5 and CYP3A4 using EDC. Holo and apo b_5 were cross-linked with CYP3A4 at 1:1 molar ratio in the absence and presence of EDC. (A) Holo b_5 and CYP3A4 reaction: lane 1, protein ladder; lane 2, holo b_5 and CYP3A4 without EDC; lane 3, holo b_5 and CYP3A4 with EDC. (B) Apo b_5 and CYP3A4 reaction: lane 1, protein ladder; lane 2, apo b_5 and CYP3A4 with EDC; lane 3, apo b_5 and CYP3A4 without EDC.

Table 1. Intermolecular Cross-Linked Peptides in the Holo b_5–CYP3A4 Complex[a]

measured monoisotopic peak (m/z)	charge state	measured peptide mass (Da)	calcd peptide mass (Da)	mass matches to intermolecular cross-linked peptides
781.40	+5	3902.00	3901.78	holo b_5 (^{48}EQAGGDATENFEDVGHSTDAR^{68})–CYP3A4 (^{92}TVLVKEC(carbamidomethyl)YSVFTNR^{105})
976.51	+4	3902.04		
744.97	+5	3719.85	3719.66	holo b_5 (^{48}EQAGGDATENFEDVGHSTDAR^{68})–CYP3A4 (^{116}SAISIAEDEEWKR^{128})
930.95	+4	3719.80		
501.29	+4	2001.16	2001.04	holo b_5 (^{35}FLEEHPGGEEVLR^{47})–CYP3A4 (^{419}FSKK^{422})

[a]The peptide digests were analyzed on an API-US quadrupole mass spectrometer (Micromass, Manchester, U.K.) as previously described.[19]

substrate concentration that gives an absorbance change of 50% of A_{max}), and n is the Hill coefficient.

Molecular Docking and Energy Minimization. The high-resolution X-ray crystallographic structure of human CYP3A4 (PDB entry 1TQN),[53] the human holo b_5 homology model made from the bovine cyt b_5 (PDB entry 1CYO) crystal structure,[54] and the rat apo b_5 NMR solution structure (PDB entry 1I87) were used to construct the model of the CYP3A4–holo/apo b_5 complexes. Manual docking of the structures was accomplished by positioning the structures, using DS Viewer Pro 6.0 (Accelrys Software Inc.), and the mass spectrometry cross-linking data as constraints. The distance between the residue pair in each identified cross-linked peptide was minimized. Some side chains of the residues on the protein interacting surfaces were reoriented using DS Viewer Pro 6.0 to avoid overlap of the side chains. The complex model was energy minimized using GROMACS (Groningen MAchine for Chemical Simulation) as previously described.[55−57] Molecular graphics and analyses were performed with the UCSF Chimera package (http://www.cgl.ucsf.edu/chimera). The intermolecular H-bonds revealed are identified through the use of the FindHBond function in Chimera.[58] Because of the ambiguous sites on apo b_5 in cross-linking with CYP3A4, the ZDOCK SERVER (http://zdock.umassmed.edu/) was used to predict the apo b_5–CYP3A4 interaction model with identified sites as constraints.[59] The complex with the lowest energy was selected as the interaction model.

Construction of Membrane Models of Holo/Apo b_5–CYP3A4 Interaction. The orientations of CYP3A4 and holo/apo b_5 relative to membranes were modeled using the method described in ref 60. The angle between the CYP3A4 heme plane and the membrane was adjusted to 58°, a value that is midway between 38° and 78° according to ref 60. The holo/apo b_5 linker domain conformation was made flexible using the software package Chimera as suggested by ref 50 and the NMR solution structure of human cyt b_5 (PDB entry 2I96).

RESULTS

Chemical Cross-Linking. The treatment of an equimolar mixture of CYP3A4 and human cyt b_5 or apo b_5 with EDC resulted in the formation of cross-linked protein complexes, with the major complex being a binary complex (cyt b_5–CYP3A4), the molecular mass of which is ~73 kDa (Figure 1). The band directly above it with a molecular mass of ~90 kDa is likely to be the (cyt b_5)$_2$–CYP3A4 complex, and other faint bands could be complexes with multiple CYPs.

Holo b_5–CYP3A4 Interactions Assessed by Mass Spectrometric Analysis. Three intermolecular cross-linked peptides of the holo b_5–CYP3A4 complex were identified with five precursor ions at different charge status (Table 1) through mass spectrometric analysis. The sequences of the three cross-linked peptide candidates were fully confirmed by the tandem mass spectra with the cross-linked residue pairs successfully located (Figure 2). In the cross-linked peptides [cyt b_5 (^{48}EQAGGDATENFEDVGHSTDAR^{58})–CYP3A4 (^{92}TVLVKECYSVFTNR^{105}) and cyt b_5 (^{48}EQAGGDATENFEDVGHSTDAR^{58})–CYP3A4 (^{116}SAISIAEDEEWKR^{128})], cross-linked sites were unambiguously determined to be Glu56 (cyt b_5)–Lys96 (CYP3A4) and Glu56 (cyt b_5)–Lys127 (CYP3A4) sites, respectively (cyt b_5 numbering according to PDB entry 1CYO). For example, on the tandem MS spectrum of the first cross-linked peptide (Figure 2A), the observation of cyt b_5 linear fragment ions such as b_8 and a series of y ions, including the longest y_{12} ions, indicates that only Glu56 can be the cross-

dx.doi.org/10.1021/bi301069r | Biochemistry 2012, 51, 9488–9500

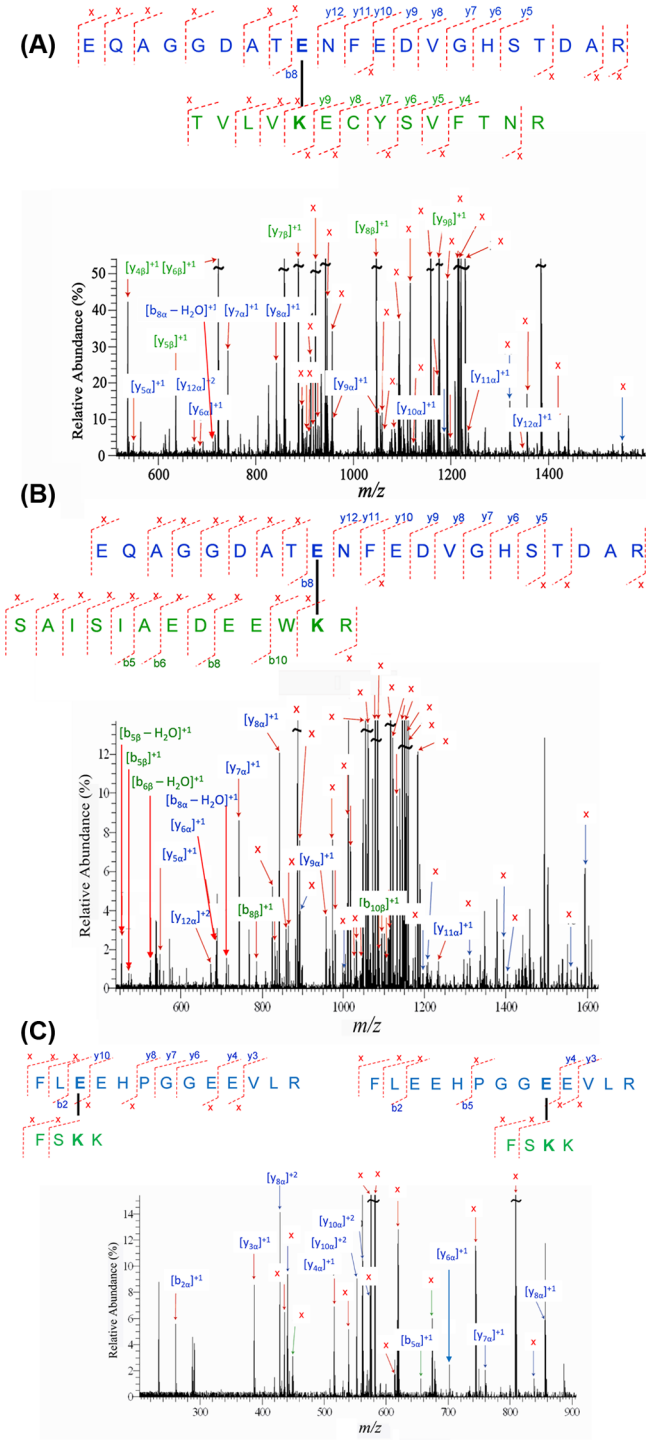

Figure 2. Tandem mass spectra for three cross-linked peptide precursor ions identified from the cyt b_5–CYP3A4 complex. Fragment ions with a superscript x represent the cross-linked fragment ions. Ions marked with a subscript α are from cyt b_5, and ions with a subscript β are from CYP3A4. Identified cross-linked residue pairs are linked by thick black lines. (A) Ion $[M + H]^{4+}$ = 976.4534 for the holo b_5 (^{48}EQAGGDATENFEDVGHSTDAR^{68})–CYP3A4 (^{92}TVLVKECYSVFTNR^{105}) complex. (B) Ion $[M + H]^{4+}$ = 930.9229 for the holo b_5 (^{48}EQAGGDATENFEDVGHSTDAR^{68})–CYP3A4 (^{116}SAISIAEDEEWKR^{128}) complex. (C) Ion $[M + H]^{4+}$ = 501.2670 for the holo b_5 (^{35}FLEEHPGGEEVLR^{47})–CYP3A4 (^{419}FSKK^{422}) complex. The measurement errors of the three ions are 0.2, 0.9, and 2.4 ppm, respectively.

linking residue. In addition, all the cross-linking fragments indicated with signal "x" agree with and further support this assignment. For the cross-linked cyt b_5 (^{35}FLEEHPGGEEVLR^{47})–CYP3A4 (^{419}FSKK^{422}) peptide, two possibilities of cross-linking sites were suggested by the spectrum (Figure 2C), Glu37 (cyt b_5)–Lys421 (CYP3A4) and Glu43 (cyt b_5)–Lys421 (CYP3A4) sites. Glu37 and Glu43 are adjacent surface residues on the structure of cyt b_5[61] and are predicted to be equally accessible to Lys421 on CYP3A4.

The two peptides on cyt b_5 identified in cross-linking with CYP3A4 contain α2–loop–α3 and α4–loop–α5 segments,[3] which form the hydrophobic core to which the heme group binds. On the other hand, the peptides on CYP3A4 contain helices B′ and C, the K″–L loop, and helix L. All three cross-linked sites are found to be on the proximal surface of CYP3A4, which has been predicted to be the redox partner binding surface for CYPs.[62,63]

Apo b_5–CYP3A4 Interactions Assessed by Mass Spectrometric Analysis. Two cross-linked peptide complexes between apo b_5 and CYP3A4 were successfully identified (Table 2). The sequences of the cross-linked peptide candidates were confirmed by their corresponding tandem mass spectra (Figure 3). The cross-linked sites on the peptide apo b_5 (^{35}FLEEHPGGEEVLR^{47})–CYP3A4 (^{116}SAISIAEDEEWKR^{128}) complex were determined to be Glu37 on apo b_5 and Lys127 on CYP3A4. On the peptide apo b_5 (^{48}EQAGGDATENFEDVGHSTDAR^{68})–CYP3A4 (^{71}VWGFYDGQQPVLAITDPDMIKTVLVK^{96}) complex, Lys91 on CYP3A4 is identified to be the cross-linked site, while further differentiation among residues Glu48, Asp53, Glu56, Glu59, and Asp60 on cyt b_5 involved in cross-linking is difficult because of the complication of the spectra and the lack of sufficient fragmentation.

Interestingly, the peptide segments identified on apo b_5 involved in cross-linking with CYP3A4 are the same as those on holo b_5 involved in cross-linking with CYP3A4, including the α2–loop–α3 and α4–loop–α5 segments (Tables 1 and 2). On CYP3A4, the Lys127 residue was identified to be cross-linked with both holo and apo b_5; the Lys91 and Lys96 residues that were identified to be cross-linked with holo/apo b_5 are very close in the three-dimensional structure of CYP3A4.

Modeling of Holo b_5–CYP3A4 and Apo b_5–CYP3A4 Complexes. Using the cross-linking sites between holo/apo b_5 and CYP3A4 as constraints and minimizing the energy of the interactions by protein docking programs, we constructed the docked models of holo/apo b_5–CYP3A4 complexes (Figure 4). For the apo b_5–CYP3A4 docking calculation, the ZDOCK server was able to calculate different combinations with the cross-linking sites as constraints, though through the tandem mass spectrum no differentiation can be made among acidic residues 48, 53, 56, 59, and 60. The model shown in Figure 4 has the lowest energy according to the docking calculation.

In both interaction models, the interacting surfaces on holo/apo b_5 include the α2–loop–α3 and α4–loop–α5 segments, with additionally one propionate group of the heme group in holo b_5 contributing to the interaction with CYP3A4. Holo b_5 and apo b_5 were predicted to bind to the same groove on CYP3A4 despite the different orientations. The contact regions on CYP3A4 for holo b_5 are predicted to be helix B, the B–B′ loop, the C–D loop, helices D, J′, and K, the K″–L meander region, the β-bulge, and helix L (Figure 4A). Those for apo b_5 are helix B, the B–B′ loop, helix C, the C–D loop, helix D, the K″–L meander region, and the β-bulge (Figure 4B). Holo b_5 and apo b_5 both approach the B–B′ loop region and helix C of

dx.doi.org/10.1021/bi301069r | Biochemistry 2012, 51, 9488–9500

Table 2. Intermolecular Cross-Linked Peptide Candidates in the Apo b_5–CYP3A4 Complex

measured monoisotopic peak (m/z)	charge state	measured peptide mass (Da)	calcd peptide mass (Da)	mass matches to intermolecular cross-linked peptides
757.3763	+4	3026.4814	3026.4854	apo b_5 (^{35}FLEEHPGGEEVLR^{47})–CYP3A4 (^{116}SAISIAEDEEWKR^{128})
606.1026	+5	3026.4812		
1024.8989	+5	5120.4627	5120.4582	apo b_5 (^{48}EQAGGDATENFEDVGHSTDAR^{68})–CYP3A4 (^{71}VWGFYDGQQPVLAITDPDMIKTVLVK^{96})

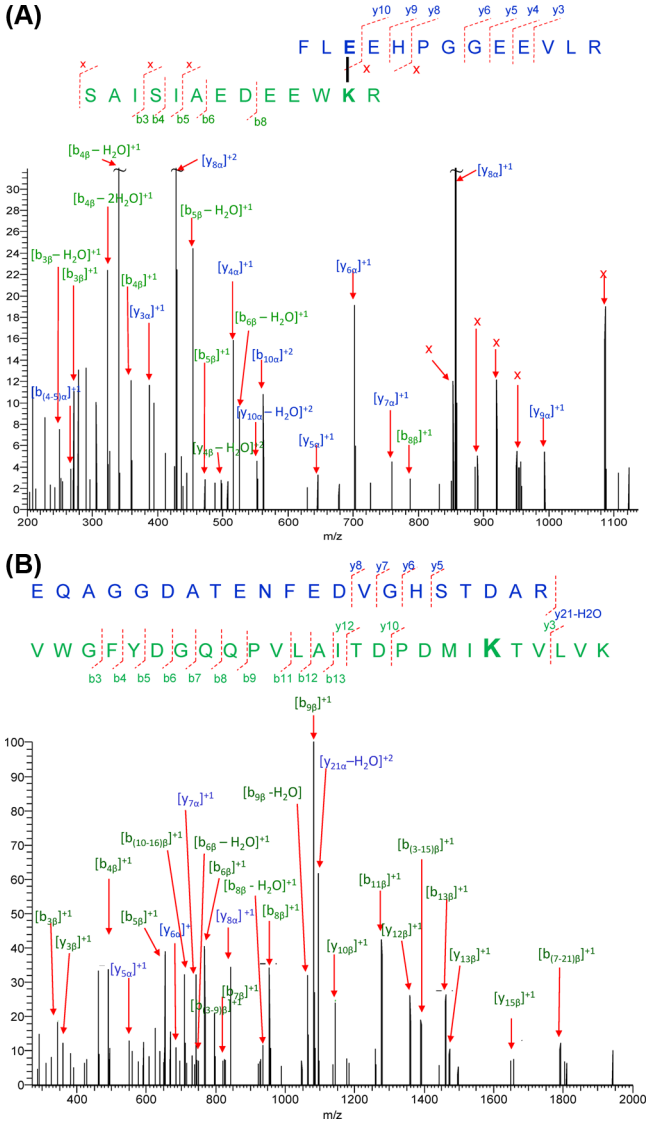

Figure 3. Tandem mass spectra for two cross-linked peptide precursor ions identified from the apo b_5–CYP3A4 complex. Fragment ions with a superscript x represent the cross-linked fragment ions. Ions marked with a subscript α are from cyt b_5, and ions with a subscript β are from CYP3A4. Identified cross-linked residue pairs are linked by thick black lines. (A) Ion $[M + H]^{4+}$ = 757.3763 for the apo b_5 (^{35}FLEEHPGGEEVLR^{47})–CYP3A4 (^{116}SAISIAEDEEWKR^{128}) complex. (B) Ion $[M + H]^{5+}$ = 1024.8989 for the apo b_5 (^{48}EQAGGDATENFEDVGHSTDAR^{68})–CYP3A4 (^{71}VWGFYDGQQPVLAITDPDMIKTVLVK^{96}) complex. The measurement errors for the two ions are 1.3 and 0.8 ppm, respectively.

CYP3A4 via helices α4 and α5, respectively. In the holo b_5–CYP3A4 model, the CYP3A4 and cyt b_5 heme groups are nearly perpendicular, and the shortest distance between the heme groups is ~11 Å.

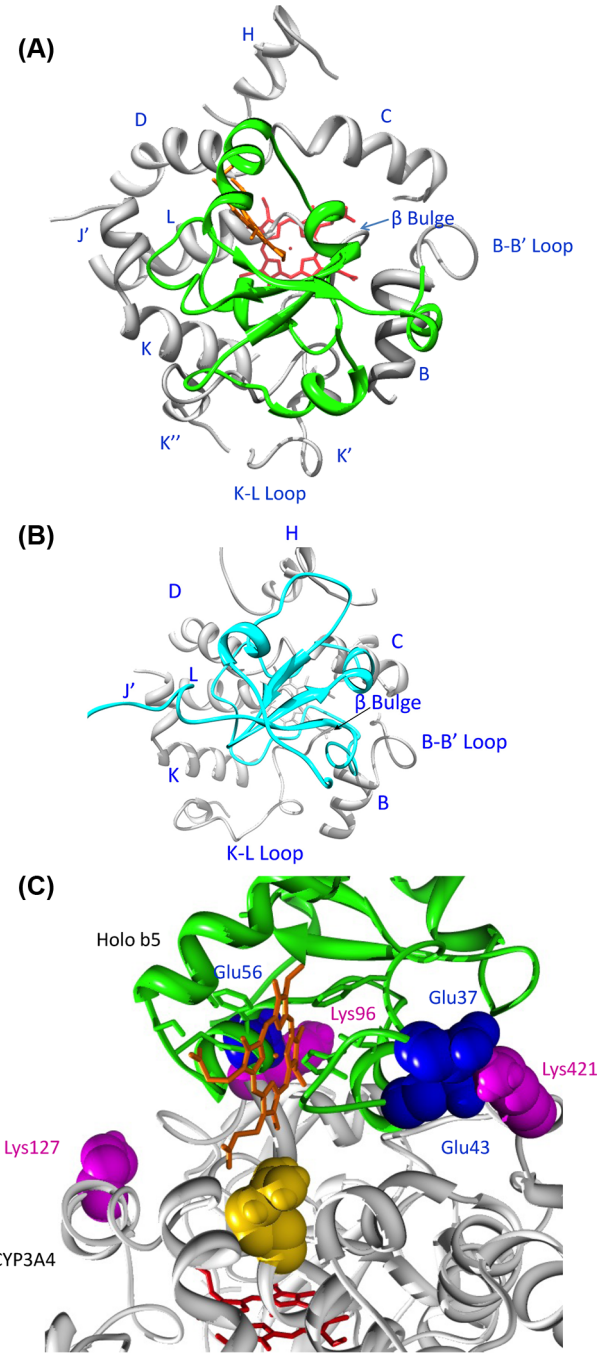

Figure 4. Holo/apo b_5–CYP3A4 complex models. CYP3A4 is colored white, cyt b_5 green, apo b_5 cyan, the heme group of CYP3A4 red, and the heme group of holo b_5 orange. The interacting residues on CYP3A4 and cyt b_5 are colored magenta and blue, respectively. Protein regions on CYP3A4 far from the interacting surfaces are truncated. (A) Top view of the holo b_5–CYP3A4 model. (B) Top view of the apo b_5–CYP3A4 model. (C) R446A (golden) illustrated in the holo b_5–CYP3A4 model.

dx.doi.org/10.1021/bi301069r | *Biochemistry* 2012, 51, 9488–9500

Table 3. Effect of the Mutations on CYP3A4 Catalytic Activities for Testosterone 6β-Hydroxylation in the Presence and Absence of Cyt b_5[a]

	with b_5		without b_5			
	V_{max} (nmol nmol of CYP3A4^{-1} min^{-1})	K_m (μM)	V_{max} (nmol nmol of CYP3A4^{-1} min^{-1})	K_m (μM)	ratio of catalytic efficiency with and without b_5	ratio of V_{max} with and without b_5
WT	27.8 ± 2.2	152.6 ± 37.5	16.4 ± 1.3	240.2 ± 48.3	2.7	1.7
K96A	16.0 ± 1.3	436.8 ± 76.0	12.6 ± 2.0	470.1 ± 149.0	1.3	1.3
K421A	16.6 ± 1.7	366.1 ± 81.4	8.3 ± 0.8	313.9 ± 73.7	1.7	2
R446A	N/A		N/A		N/A	N/A
triple mutant	N/A		N/A		N/A	N/A

[a]Each point represents the mean ± SD (n = 3). N/A means not available.

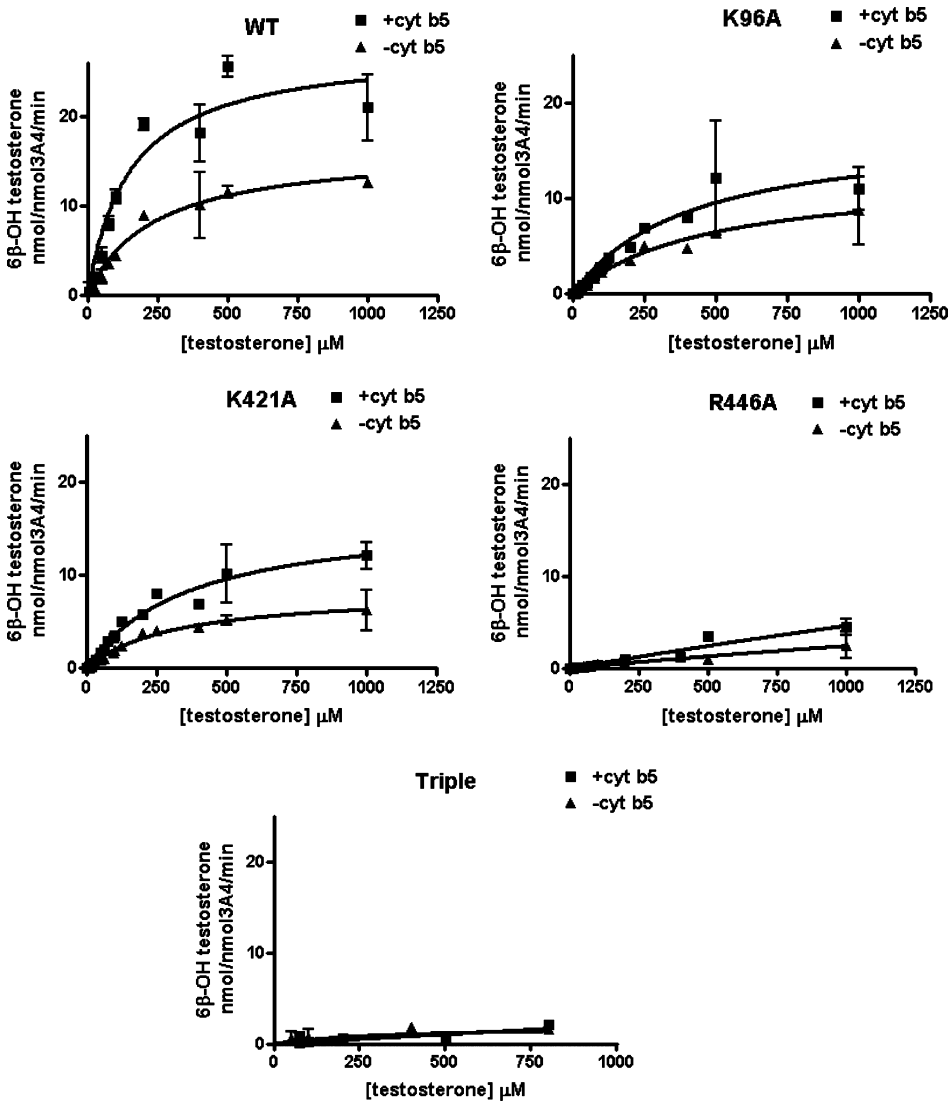

Figure 5. NADPH-dependent formation of 6β-hydroxytestosterone by CYP3A4 and its mutants. Reactions were conducted using 40 pmol of CYP3A4, 80 pmol of CPR, and 40 pmol of b_5, in a 200 μL reaction volume for 10 min. Each point represents the mean ± SD (n = 3).

Site-Directed Mutagenesis of CYP3A4. To confirm the biological function of the residues on CYP3A4 identified by the cross-linking study, we conducted site-directed single-point and multiple substitutions of the three Lys residues of CYP3A4 (Lys96, Lys127, and Lys421) to Ala. In addition, Arg446 was included in the mutagenesis study, because this residue was at the interface of the holo b_5–CYP3A4 complex model and therefore was predicted to be of significance for cyt b_5 interaction. It was postulated that the interactions between CYP3A4 and cyt b_5 initiated by electrostatic interaction would be affected by substitution of the basic Lys residues with neutral Ala.

The purified CYP3A4 single-point mutations K96A, K421A, and R446A and triple mutation K96A/K127A/K421A all showed homogeneous 450 nm peaks in the reduced carbon monoxide binding difference spectrum (Figure S1 of the Supporting Information). The expression level of K127A was extremely low for unknown reasons, so it was not further

dx.doi.org/10.1021/bi301069r | Biochemistry 2012, 51, 9488–9500

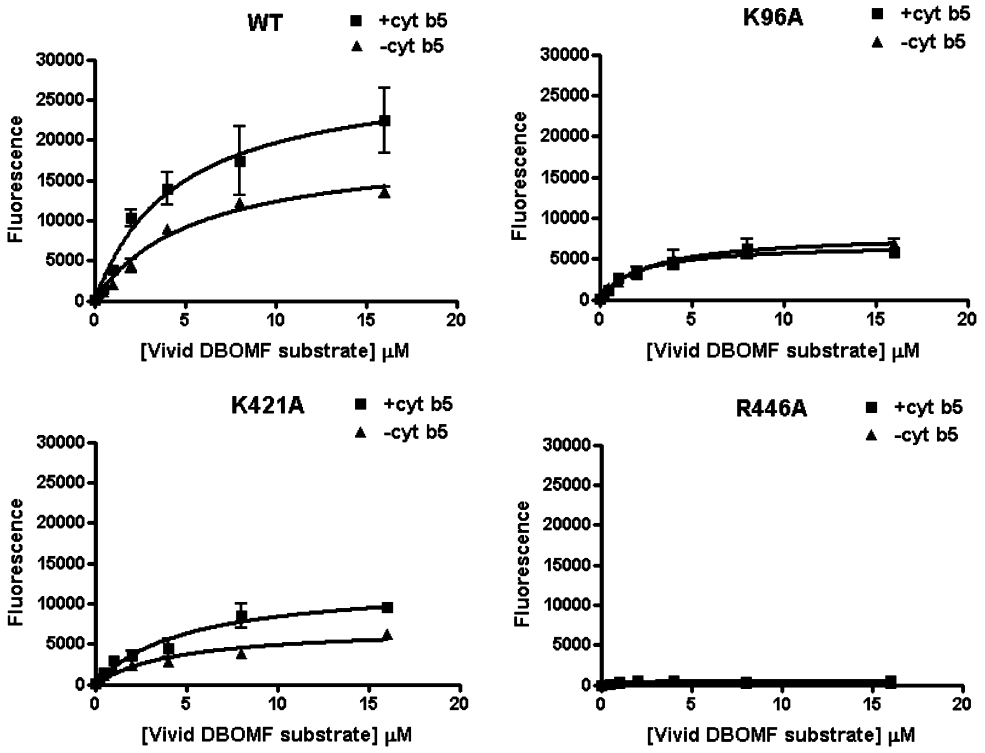

Figure 6. NADPH-dependent formation of Vivid Green from Vivid DBOMF by CYP3A4 and its mutants. Reactions were conducted using 40 pmol of CYP3A4/mutation, 80 pmol of CPR, and 40 pmol of b_5, in a 200 μL reaction volume for 15 min. Each point represents the mean ± SD (n = 3).

studied. To determine whether their active sites had been affected by the mutations, a testosterone binding affinity assay was conducted (Figure S2 of the Supporting Information). Analysis of the data using the Hill equation yielded $K_{d(app)}$ (or S_{50}) values of 25 ± 12 μM (N = 1.53; R^2 = 0.99), 71 ± 28 μM (N = 1.45; R^2 = 0.99), 108 ± 34 μM (N = 1.07; R^2 = 0.995), 30 ± 8 μM (N = 1.34; R^2 = 0.997), and 42 ± 25 μM (N = 1.31; R^2 = 0.99) for wild-type CYP3A4, K96A, K421A, R446A, and the triple mutant, respectively. The wild-type apparent dissociation constant is comparable to that previously reported.[51,52] All mutated proteins bind to testosterone with apparent K_d values in a range of 1−4-fold of that of the wild type, suggesting that the active sites of the mutations were modestly altered by the mutations. Also, the data indicate that the TST induces smaller-magnitude spin state changes for the mutants compared to the wild type. Presumably, these mutations affect the conformation of either the substrate free enzyme or the ligand-bound complexes and thus have an impact on the energetics and solvent effects of substrate binding. Specifically for K421A, the mutation site is at the K−L loop, partly involved in channel 5 of CYP3A4's substrate access−egress channel; however, this channel 5 (between K and K′ to the active site) has been found not to open during the computer dynamic simulations of CYP3A4.[64,65] An important result of these studies is that the mutations do not significantly impair TST binding, which can, therefore, be used to probe the effects of these residues on cyt b_5 binding and catalysis in the presence of CPR.

Effect of the Mutations on the Catalytic Activities of CYP3A4. TST 6β-hydroxylation, a probe reaction of CYP3A4, was used to measure the activities of wild-type CYP3A4 and the mutants. The stimulatory effects of cyt b_5 on these enzymes were compared, as shown in Table 3 and Figure 5 for a single concentration of cyt b_5, with a 1:2:1 CYP:CPR:cyt b_5 ratio. The catalytic efficiency (V_{max}/K_m) of wild-type CYP3A4, K421A, and K96A was increased by cyt b_5 2.7-, 1.7-, and 1.3-fold, respectively, under these conditions. The V_{max} ratios with and without b_5 are 1.7, 1.3, and 2, respectively. The results indicate a complex effect of the cyt b_5 dependence on both V_{max} and K_m terms for TST hydroxylation. These results indicate that the Lys96 residue likely plays a more important role than Lys421 in the functional interaction of CYP3A4 with cyt b_5. Interestingly, the triple mutant K96A/K127A/K421A displayed very low catalytic activity in the absence and presence of cyt b_5. That is, simultaneous substitution of the three sites depleted the activity of CYP3A4. It is remarkable that the R446A mutation also completely abolished CYP3A4 activity. Another probe of CYP3A4, fluorogenic Vivid 3A4 substrate DBOMF, was also tested for activities of wild-type CYP3A4 and its mutants (Figure 6). The results were very consistent with testosterone 6β-hydroxylation activities. Overall, the mutagenesis study confirmed the functional importance of the ion pairs identified by the cross-linking study.

Effect of the Mutations on the Binding of CYP3A4 to Cyt b_5. The catalytic experiments do not explicitly distinguish between the effects of the mutations on cyt b_5 binding versus cyt b_5-dependent interactions with TST. To further examine the effect of the mutations on the binding of cyt b_5 to CYP3A4, the affinity of cyt b_5 for wild-type CYP3A4 and its mutants was measured using a spectral titration method.[66,67] As shown in Figure 7, cyt b_5 bound to wild-type CYP3A4, K96A, and K421A with estimated K_d values of 140 ± 37, 346 ± 198, and 287 ± 37 nM, respectively. This suggests that effects of mutations observed in functional studies may in part be due to the altered affinity of the protein interactions. The studies do not, however, clarify any specific molecular mechanism by which mutation affects K_M versus V_{max} in the functional studies. The binding affinity of cyt b_5 with R446A was drastically decreased

dx.doi.org/10.1021/bi301069r | Biochemistry 2012, 51, 9488−9500

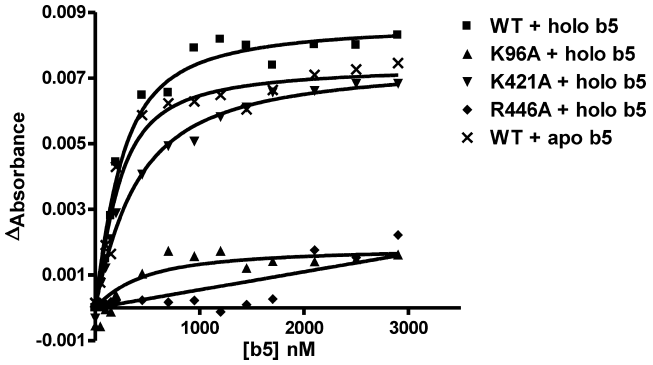

Figure 7. Titration of cyt b_5 to wild-type CYP3A4 and its mutants and apo b_5 to wild-type CYP3A4. The spectral titration experiment was conducted using 200 nM CYP3A4 or mutants and titration with cyt b_5 or apo b_5. The magnitude of the absorbance change at 390 nm minus that at 418 nm was measured following each addition of cyt b_5 at room temperature.

as indicated by the binding assay, with a K_d value estimated to be >1000 μM.

It has been reported that the ratio of cyt b_5 to CYP can affect the CYP catalytic rate, as cyt b_5 competes with CPR for the partially overlapping binding sites on CYPs.[15,68,69] Results in Figure 8 reveal a ratio-dependent effect of cyt b_5 on CYP3A4

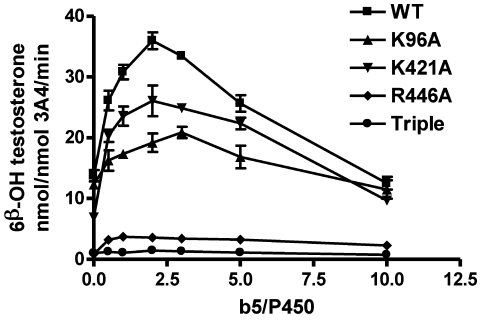

Figure 8. Effect of the cyt b_5:CYP ratio on the formation of 6β-hydroxytestosterone by CYP3A4 and its mutants. Reactions were conducted using varying concentrations of cyt b_5 and a constant ratio of CYP3A4 (40 pmol) to CPR (80 pmol) for 10 min in a 200 μL reaction volume. Each point represents the mean ± SD (n = 3).

activities, with a stimulatory effect at low ratios, but an inhibitory effect with increasing b_5:CYP3A4 ratios. Both wild-type CYP3A4 and K421A have their maximal activities at a ratio of 2:1. K96A reached its highest activity at a b_5:CYP3A4 ratio of 3:1, which is consistent with previous cyt b_5 binding assays with the mutated protein. Expectedly, both the triple mutant and R446A showed very low activity in the presence or absence of cyt b_5.

Effect of the Mutations on the Interaction of CYP3A4 with CPR. Because CPR is expected to share sites of interaction on CYP with cyt b_5, the effects of the mutations on CYP3A4 activity in the presence of varying concentrations of CPR were determined. TST 6β-hydroxylation, dependent on CPR concentrations, exhibited Michaelis–Menten kinetics; therefore, the apparent $K'_{m,CPR}$ was used to illustrate the affinity of the CYP3A4–CPR interaction.[49,70] As shown in Figure 9, wild-type CYP3A4, K96A, and K421A have comparable binding $K'_{m,CPR}$ values (41 ± 10, 91 ± 21, and 70 ± 12 nM, respectively). CPR binding to R446A and the triple mutant was

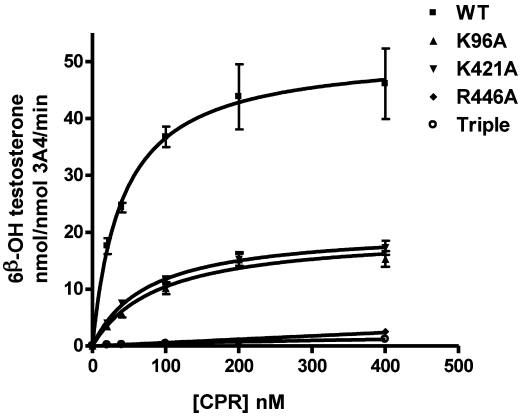

Figure 9. Effect of the CPR:CYP ratio on the formation of 6β-hydroxytestosterone by CYP3A4 and its mutations. Reactions were conducted using varying concentrations of CPR and a constant ratio of CYP3A4 (40 pmol) to cyt b_5 (40 pmol) for 10 min in a 200 μL reaction volume. Each point represents the mean ± SD (n = 3).

abolished. The apparent binding of CPR to CYP3A4 and mutant CYP3A4 agrees with the earlier proposal that cyt b_5 and CPR have overlapped binding sites on P450s and they compete with each other for binding to P450s.[63,69,71]

DISCUSSION

This investigation of the role of intersurface residues in the holo/apo b_5–CYP3A4 complex provides information about the structural organization of the complexes and supports the allosteric roles of holo/apo b_5 in modulating the catalytic efficiency of CYP3A4. Apo b_5 and holo b_5 interact with overlapping sites on CYP3A4, with different orientations. Both directly contact the B–B′ loop region of CYP3A4, one of the major substrate recognition sites (SRSs) of CYP3A4.[72] Previous studies have shown that lapachenole, a substrate of CYP3A4, covalently binds to this loop region.[73] This loop region is also found to be highly flexible by computer dynamics simulations.[64,74] Thus, it is reasonable to postulate that the contact of cyt b_5 with CYP3A4 can induce conformational changes in this structural element. The induction of conformational changes of CYP enzymes has been observed in $P450_{cam}$ (CYP101) upon cyt b_5 binding, whose structural perturbations happened not only to the proximal surface structural elements, including helices B and C, but also to those in the distal surface, including regions for substrate access and orientation.[75] Consequently, it is reasonable to extrapolate that association of CYP3A4 with cyt b_5, even in the absence of effects on rates of reduction of intermediates in the CYP reaction cycle, can give rise to the allosteric effect on it. This allosteric effect is further supported by apo b_5 exhibiting a stimulatory effect on CYP3A4 (Table 4 and refs 8 and 9).

The interaction sites of the holo/apo b_5–CYP3A4 complex are also found to be consistent with their membrane-associated

Table 4. Comparison of the Effects of Modulation of Holo b_5 and Apo b_5 on CYP3A4 Catalytic Activities[a]

CYP3A4	V_{max} (nmol nmol of CYP3A4^{-1} min^{-1})
with holo b_5	22.7 ± 0.4
with apo b_5	17.7 ± 2.6
−cyt b_5	12.9 ± 1.0

[a]Each point represents the mean ± SD (n = 3).

dx.doi.org/10.1021/bi301069r | Biochemistry 2012, 51, 9488–9500

models under physiological conditions as in Figure 10. CYPs are embedded in the membrane by an N-terminal membrane anchor and the F−G loop,[60,76] with 38−78° angles between the heme plane and the membrane plane[60] depending on the CYP isoform. Cyt b_5 has a flexible 15-amino acid linker domain between its cytosolic functional domain and the C-terminal transmembrane domain, which facilitates appropriate positions of the functional domain to interact with CYPs effectively.[50,77] The relative positions of CYP3A4 and cyt b_5 shown in Figure 10 indicate that under physiological conditions, holo and apo b_5 are able to adopt orientations consistent with the models based on our cross-linking constraints to interact with CYP3A4 effectively.

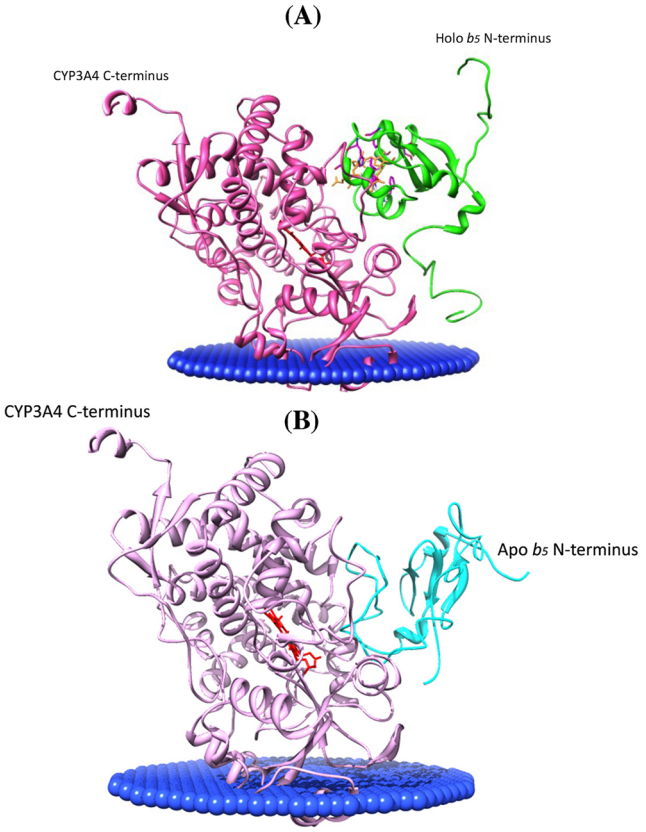

Figure 10. Orientations of CYP3A4 and holo/apo b_5 in membranes. The angle between the CYP3A4 heme (red) plane and the membrane slab (blue) was adjusted to 58°, a value between 38° and 78° according to ref 60. The holo and apo b_5 linker domain conformation was made flexible according to ref 50 as well as the human and rabbit cyt b_5 NMR structure (PDB entry 2I96). CYP3A4 is colored light purple, holo b_5 green, and apo b_5 cyan. (A) Holo b_5−CYP3A4 interaction model position relative to the membrane. (B) Apo b_5−CYP3A4 interaction model position relative to the membrane.

A comparison of the structural elements on CYP2E1 that interacts with cyt b_5 is useful. Our laboratory previously characterized holo b_5−CYP2E1 interaction, and it is enlightening to compare the current holo b_5−CYP3A4 model with it. In the holo b_5−CYP2E1 interaction model, the heme groups of cyt b_5 and CYP2E1 that were involved in the contacts were predicted to be in an orientation consistent with its electron transfer role for CYP2E1 catalysis.[19] It is worth noting that the acidic residues on cyt b_5 at the interacting surface, which are negatively charged under physiological conditions, are conserved across species.[3] In contrast, the distribution of charged residues on the surfaces of CYP2E1 and CYP3A4 varies because of the diversity of CYP isoforms. Thus, driven by electrostatic forces, cyt b_5 can position itself differently in binding to CYP3A4 and CYP2E1.[19] This different orientation of cyt b_5 in binding to different CYPs could account for its CYP isoform-dependent effect. Comparison of the cyt b_5−CYP3A4 and cyt b_5−CYP2E1 complexes[19] reveals very significant differences in binding features. Helix J′ found in the CYP2E1−cyt b_5 interaction does not exist in the cyt b_5−CYP3A4 complex. On the other hand, interacting helices B, D, and K″ of CYP3A4 were not seen in the cyt b_5−CYP2E1 complex. Most significantly, the B−B′ loop of CYP3A4, a well-recognized SRS, makes contact with helices α3 and α4 surrounding the heme group of cyt b_5. This specific interaction between cyt b_5 and the CYP2E1 B−B′ loop does not exist in the model. Therefore, cyt b_5 does not exert a major allosteric effect on CYP2E1 as it does on CYP3A4.

Functional studies (Figures 5 and 6) using both a classical substrate, testosterone, and a fluorogenic Vivid CYP3A4 substrate confirmed that the cross-linking sites identified by mass spectrometry study are important for cyt b_5 and CYP catalysis. Mutation of Lys96 had a greater impact on the stimulatatory effect of cyt b_5 on CYP3A4 than that of Lys421, in parallel with the lower binding affinity of cyt b_5 with K96A versus that with K421A. The affinity of the apo b_5−CYP3A4 complex is similar to that of the holo b_5−CYP3A4 complex (Figure 7), consistent with the similar stimulatory effects of holo b_5 and cyt b_5 on CYP3A4 activity, which can be explained by our models of their interactions; the models showed that the holo and apo b_5−CYP3A4 complexes both bind to the same groove on CYP3A4, albeit with a different orientation.

The experiment with varying cyt b_5:CYP3A4 ratio suggests that cyt b_5 and CPR have overlapping binding sites on CYPs and compete with each other to bind to CYPs[71] (Figure 8). At higher cyt b_5:CYP3A4 ratios, CYP3A4 activity was decreased compared with that stimulated at lower ratios. Similar observations were also reported by Locuson et al., who found that at high cyt b_5:CYP2C9 ratios (>4), the oxidase activity was decreased[15] and proposed that competition between CPR and cyt b_5 at very high concentrations of cyt b_5 would weaken the essential binding of CPR and slow the transfer of electrons from NADPH, therefore resulting in a decrease in overall oxidase activity. In our study, when the cyt b_5:CYP3A4 ratio is varied, at a 3:1 ratio K96A showed maximal catalytic activity. The stimulatory effects on K96A catalytic efficiency are slightly lower than those for K421A, possibly because of the higher K_d value of cyt b_5 with K96A versus that with K421A (Figure 7), because CPR has a comparable affinity with both K96A and K421A. Noting that there is still strong binding of cyt b_5 to the single-point mutation, the study also suggests that the sum of different kinds of interactions, e.g., electrostatic and weak hydrophobic interactions, altogether makes decisive contributions to functional cyt b_5−CYP3A4 interaction.

The triple (K96A/K127A/K421A) mutation exhibited only minimal activity in metabolizing either TST or Vivid 3A4 substrate. The triple mutation was, therefore, not considered in further functional studies. As mentioned previously, both K96A and K421A retained CPR binding capability and catalytic activity for both substrates; we therefore suspected that Lys127 might be more important in CPR−CYP3A4 binding. Alternatively, the three sites synergistically play a pivotal role in CPR−CYP3A4 binding. R446A exhibited a dramatic decrease in its activity, indicating the importance of this

dx.doi.org/10.1021/bi301069r | Biochemistry 2012, 51, 9488−9500

residue in interacting with CPR, an essential redox partner of P450. In the holo b_5−CYP3A4 interaction models, Arg446 appeared to be in close contact with the binding partners. Arg446 was found to be conserved among human CYP species such as 2A6, 2C19, 2D6, 2E1, 3A5, and 2J2. Earlier studies of rabbit CYP2B4 showed that Arg443 (equivalent to Arg446 in CYP3A4) on CYP2B4 contributes to CPR binding.[40]

In conclusion, in this study, we identified the interaction surfaces of both holo and apo b_5 with CYP3A4 using chemical cross-linking coupled with mass spectrometric analysis and determined the functional importance of the interacting residues on CYP3A4 using site-directed mutagenesis and metabolic assays. Computer models of both the holo and apo b_5−CYP3A4 complexes were constructed for the first time at the atomic level, which illustrated the similarities and differences in the interaction of holo and apo b_5 with CYP3A4. To the extent that apo b_5 binds at the same surface as holo b_5 and activates CYP3A4 activity, the results support the possibility that cyt b_5 plays an allosteric role in CYP3A4 catalytic activity, in addition to possible electron transfer by the holoprotein. The critical role of Arg446 on CYP3A4 in the interaction with both cyt b_5 and CPR is also suggested. These findings provide further insight into the complex mechanisms of cyt b_5 modulation of CYPs.

■ ASSOCIATED CONTENT

Supporting Information

CYP3A4 mutant CO binding difference spectra, and TST binding spectra. This material is available free of charge via the Internet at http://pubs.acs.org.

Accession Codes

Protein Data Bank entries 1TQN, 1CYO, and 1I87.

■ AUTHOR INFORMATION

Corresponding Author

*Telephone: (206) 685-0379. Fax: (206) 685-3252. E-mail: winky@u.washington.edu.

Author Contributions

The manuscript was written through contributions of all authors. All authors have given approval to the final version of the manuscript.

Funding

This work was supported by National Institute of General Medical Sciences Program Project Grant GM32165. This work was also supported in part by the University of Washington's Proteomics Resource (UWPR95794).

Notes

The authors declare no competing financial interest.

■ ACKNOWLEDGMENTS

We thank Dr. Priska D. von Haller and Dr. Michael J. Dabrowski for their kind help and the Collaboratory for MS3D Portal sponsored by the National Institutes of Health and the National Science Foundation and are grateful for the Chimera package developed by the Resource for Biocomputing, Visualization, and Informatics at the University of California, San Francisco. Finally, this work is dedicated to the Memory of Professor Sid Nelson, who will be missed.

■ ABBREVIATIONS

CYP, cytochrome P450; cyt b_5 or holo b_5, cytochrome b_5; apo b_5, cyt b_5 devoid of heme; SRS, substrate recognition sites; CPR, cytochrome P450 reductase; EDC, reagent 1-ethyl-3-[3-(dimethylamino)propyl]carbodiimide hydrochloride; IPTG, isopropyl β-D-1-thiogalactopyranoside; δ-ALA, 5-aminolevulinic acid; IAM, 2-iodoacetamide; DTT, dithiothreitol; DLPC, L-α-dilauroyl-*sn*-glycero-3-phosphocholine; DOPC, L-α-dioleoyl-*sn*-glycero-3-phosphocholine; DLPS, L-α-dilauroyl-*sn*-glycero-3-phosphoserine; GSH, glutathione; HEPES, 4-(2-hydroxyethyl)-1-piperazineethanesulfonic acid; BME, β-mercaptoethanol; TST, testosterone; PDB, Protein Data Bank; SD, standard deviation.

■ REFERENCES

(1) Ortiz de Montellano, P. R. (2005) *Cytochrome P450: Structure, Mechanism, and Biochemistry*, Kluwer Academic, New York.

(2) Porter, T. D. (2002) The roles of cytochrome b5 in cytochrome P450 reactions. *J. Biochem. Mol. Toxicol. 16*, 311−316.

(3) Schenkman, J. B., and Jansson, I. (2003) The many roles of cytochrome b5. *Pharmacol. Ther. 97*, 139−152.

(4) Vatsis, K. P., Theoharides, A. D., Kupfer, D., and Coon, M. J. (1982) Hydroxylation of prostaglandins by inducible isozymes of rabbit liver microsomal cytochrome P-450. Participation of cytochrome b5. *J. Biol. Chem. 257*, 11221−11229.

(5) Yamazaki, H., Johnson, W. W., Ueng, Y. F., Shimada, T., and Guengerich, F. P. (1996) Lack of electron transfer from cytochrome b5 in stimulation of catalytic activities of cytochrome P450 3A4. Characterization of a reconstituted cytochrome P450 3A4/NADPH-cytochrome P450 reductase system and studies with apo-cytochrome b5. *J. Biol. Chem. 271*, 27438−27444.

(6) Kuwahara, S., and Omura, T. (1980) Different requirement for cytochrome b5 in NADPH-supported O-deethylation of p-nitrophenetole catalyzed by two types of microsomal cytochrome P-450. *Biochem. Biophys. Res. Commun. 96*, 1562−1568.

(7) Loughran, P. A., Roman, L. J., Miller, R. T., and Masters, B. S. (2001) The kinetic and spectral characterization of the *E. coli*-expressed mammalian CYP4A7: Cytochrome b5 effects vary with substrate. *Arch. Biochem. Biophys. 385*, 311−321.

(8) Yamazaki, H., Gillam, E. M., Dong, M. S., Johnson, W. W., Guengerich, F. P., and Shimada, T. (1997) Reconstitution of recombinant cytochrome P450 2C10(2C9) and comparison with cytochrome P450 3A4 and other forms: Effects of cytochrome P450-P450 and cytochrome P450-b5 interactions. *Arch. Biochem. Biophys. 342*, 329−337.

(9) Yamazaki, H., Nakamura, M., Komatsu, T., Ohyama, K., Hatanaka, N., Asahi, S., Shimada, N., Guengerich, F. P., Shimada, T., Nakajima, M., and Yokoi, T. (2002) Roles of NADPH-P450 reductase and apo- and holo-cytochrome b5 on xenobiotic oxidations catalyzed by 12 recombinant human cytochrome P450s expressed in membranes of *Escherichia coli*. *Protein Expression Purif. 24*, 329−337.

(10) Morgan, E. T., and Coon, M. J. (1984) Effects of cytochrome b5 on cytochrome P-450-catalyzed reactions. Studies with manganese-substituted cytochrome b5. *Drug Metab. Dispos. 12*, 358−364.

(11) Gruenke, L. D., Konopka, K., Cadieu, M., and Waskell, L. (1995) The stoichiometry of the cytochrome P-450-catalyzed metabolism of methoxyflurane and benzphetamine in the presence and absence of cytochrome b5. *J. Biol. Chem. 270*, 24707−24718.

(12) Hildebrandt, A., and Estabrook, R. W. (1971) Evidence for the participation of cytochrome b_5 in hepatic microsomal mixed-function oxidation reactions. *Arch. Biochem. Biophys. 143*, 66−79.

(13) Bonfils, C., Balny, C., and Maurel, P. (1981) Direct evidence for electron transfer from ferrous cytochrome b_5 to the oxyferrous intermediate of liver microsomal cytochrome P-450 LM2. *J. Biol. Chem. 256*, 9457−9465.

(14) Schenkman, J. B., Voznesensky, A. I., and Jansson, I. (1994) Influence of ionic strength on the P450 monooxygenase reaction and role of cytochrome b_5 in the process. *Arch. Biochem. Biophys. 314*, 234−241.

(15) Locuson, C. W., Wienkers, L. C., Jones, J. P., and Tracy, T. S. (2007) CYP2C9 protein interactions with cytochrome b_5: Effects on the coupling of catalysis. *Drug Metab. Dispos. 35*, 1174−1181.
(16) Gilep, A. A., Guryev, O. L., Usanov, S. A., and Estabrook, R. W. (2001) Apo-cytochrome b5 as an indicator of changes in heme accessability: Preliminary studies with cytochrome P450 3A4. *J. Inorg. Biochem. 87*, 237−244.
(17) Tamburini, P. P., MacFarquhar, S., and Schenkman, J. B. (1986) Evidence of binary complex formations between cytochrome P-450, cytochrome b5, and NADPH-cytochrome P-450 reductase of hepatic microsomes. *Biochem. Biophys. Res. Commun. 134*, 519−526.
(18) Rodgers, K. K., and Sligar, S. G. (1991) Mapping electrostatic interactions in macromolecular associations. *J. Mol. Biol. 221*, 1453−1460.
(19) Gao, Q., Doneanu, C. E., Shaffer, S. A., Adman, E. T., Goodlett, D. R., and Nelson, S. D. (2006) Identification of the interactions between cytochrome P450 2E1 and cytochrome b5 by mass spectrometry and site-directed mutagenesis. *J. Biol. Chem. 281*, 20404−20417.
(20) Chen, W., Koenigs, L. L., Thompson, S. J., Peter, R. M., Rettie, A. E., Trager, W. F., and Nelson, S. D. (1998) Oxidation of acetaminophen to its toxic quinone imine and nontoxic catechol metabolites by baculovirus-expressed and purified human cytochromes P450 2E1 and 2A6. *Chem. Res. Toxicol. 11*, 295−301.
(21) Di Primo, C., Deprez, E., Sligar, S. G., and Hui Bon Hoa, G. (1997) Origin of the photoacoustic signal in cytochrome P-450cam: Role of the Arg186-Asp251-Lys178 bifurcated salt bridge. *Biochemistry 36*, 112−118.
(22) Yamazaki, H., Shimada, T., Martin, M. V., and Guengerich, F. P. (2001) Stimulation of cytochrome P450 reactions by apo-cytochrome b_5: evidence against transfer of heme from cytochrome P450 3A4 to apo-cytochrome b_5 or heme oxygenase. *J. Biol. Chem. 276*, 30885−30891.
(23) Kumar, S., Davydov, D. R., and Halpert, J. R. (2005) Role of cytochrome b_5 in modulating peroxide-supported CYP3A4 activity: evidence for a conformational transition and cytochrome P450 heterogeneity. *Drug. Metab. Dispos. 33*, 1131−1136.
(24) Yamazaki, H., Nakano, M., Gillam, E. M., Bell, L. C., Guengerich, F. P., and Shimada, T. (1996) Requirements for cytochrome b_5 in the oxidation of 7-ethoxycoumarin, chlorzoxazone, aniline, and N-nitrosodimethylamine by recombinant cytochrome P450 2E1 and by human liver microsomes. *Biochem. Pharmacol. 52*, 301−309.
(25) Moore, C. D., al-Misky, O. N., and Lecomte, J. T. (1991) Similarities in structure between holocytochrome b5 and apocytochrome b5: NMR studies of the histidine residues. *Biochemistry 30*, 8357−8365.
(26) Moore, C. D., and Lecomte, J. T. (1990) Structural properties of apocytochrome b5: Presence of a stable native core. *Biochemistry 29*, 1984−1989.
(27) Moore, C. D., and Lecomte, J. T. (1993) Characterization of an independent structural unit in apocytochrome b5. *Biochemistry 32*, 199−207.
(28) Schrag, M. L., and Wienkers, L. C. (2001) Triazolam substrate inhibition: evidence of competition for heme-bound reactive oxygen within the CYP3A4 active site. *Adv. Exp. Med. Biol. 500*, 347−350.
(29) Jushchyshyn, M. I., Hutzler, J. M., Schrag, M. L., and Wienkers, L. C. (2005) Catalytic turnover of pyrene by CYP3A4: evidence that cytochrome b_5 directly induces positive cooperativity. *Arch. Biochem. Biophys. 438*, 21−28.
(30) Yamaguchi, Y., Khan, K. K., He, Y. A., He, Y. Q., and Halpert, J. R. (2004) Topological changes in the CYP3A4 active site probed with phenyldiazene: effect of interaction with NADPH-cytochrome P450 reductase and cytochrome b_5 and of site-directed mutagenesis. *Drug Metab. Dispos. 32*, 155−161.
(31) Guryev, O. L., Gilep, A. A., Usanov, S. A., and Estabrook, R. W. (2001) Interaction of apo-cytochrome b_5 with cytochromes P4503A4 and P45017A: relevance of heme transfer reactions. *Biochemistry 40*, 5018−5031.
(32) Holmans, P. L., Shet, M. S., Martin-Wixtrom, C. A., Fisher, C. W., and Estabrook, R. W. (1994) The high-level expression in *Escherichia coli* of the membrane-bound form of human and rat cytochrome b_5 and studies on their mechanism of function. *Arch. Biochem. Biophys. 312*, 554−565.
(33) Gillam, E. M., Baba, T., Kim, B. R., Ohmori, S., and Guengerich, F. P. (1993) Expression of modified human cytochrome P450 3A4 in *Escherichia coli* and purification and reconstitution of the enzyme. *Arch. Biochem. Biophys. 305*, 123−131.
(34) Woods, C. M., Fernandez, C., Kunze, K. L., and Atkins, W. M. (2011) Allosteric activation of cytochrome P450 3A4 by α-naphthoflavone: Branch point regulation revealed by isotope dilution analysis. *Biochemistry 50*, 10041−10051.
(35) Strittmatter, P. (1960) The nature of the heme binding in microsomal cytochrome b_5. *J. Biol. Chem. 235*, 2492−2497.
(36) Naffin-Olivos, J. L., and Auchus, R. J. (2006) Human cytochrome b5 requires residues E48 and E49 to stimulate the 17,20-lyase activity of cytochrome P450c17. *Biochemistry 45*, 755−762.
(37) Shen, A. L., Christensen, M. J., and Kasper, C. B. (1991) NADPH-cytochrome P-450 oxidoreductase. The role of cysteine 566 in catalysis and cofactor binding. *J. Biol. Chem. 266*, 19976−19980.
(38) Shen, A. L., Porter, T. D., Wilson, T. E., and Kasper, C. B. (1989) Structural analysis of the FMN binding domain of NADPH-cytochrome P-450 oxidoreductase by site-directed mutagenesis. *J. Biol. Chem. 264*, 7584−7589.
(39) Schenkman, J. B., and Jansson, I. (1999) Interactions between cytochrome P450 and cytochrome b_5. *Drug Metab. Rev. 31*, 351−364.
(40) Bridges, A., Gruenke, L., Chang, Y. T., Vakser, I. A., Loew, G., and Waskell, L. (1998) Identification of the binding site on cytochrome P450 2B4 for cytochrome b_5 and cytochrome P450 reductase. *J. Biol. Chem. 273*, 17036−17049.
(41) Hlavica, P., Schulze, J., and Lewis, D. F. (2003) Functional interaction of cytochrome P450 with its redox partners: a critical assessment and update of the topology of predicted contact regions. *J. Inorg. Biochem. 96*, 279−297.
(42) Grabarek, Z., and Gergely, J. (1990) Zero-length crosslinking procedure with the use of active esters. *Anal. Biochem. 185*, 131−135.
(43) Mosher, C. M., Tai, G., and Rettie, A. E. (2009) CYP2C9 amino acid residues influencing phenytoin turnover and metabolite regio- and stereochemistry. *J. Pharmacol. Exp. Ther. 329*, 938−944.
(44) Ye, X., Luke, B., Andresson, T., and Blonder, J. (2009) ^{18}O stable isotope labeling in MS-based proteomics. *Brief. Funct. Genomic. Proteomic. 8*, 136−144.
(45) Singh, P., Shaffer, S. A., Scherl, A., Holman, C., Pfuetzner, R. A., Larson Freeman, T. J., Miller, S. I., Hernandez, P., Appel, R. D., and Goodlett, D. R. (2008) Characterization of protein cross-links via mass spectrometry and an open-modification search strategy. *Anal. Chem. 80*, 8799−8806.
(46) Schilling, B., Row, R. H., Gibson, B. W., Guo, X., and Young, M. M. (2003) MS2Assign, automated assignment and nomenclature of tandem mass spectra of chemically crosslinked peptides. *J. Am. Soc. Mass Spectrom. 14*, 834−850.
(47) Yu, E. T., Hawkins, A., Kuntz, I. D., Rahn, L. A., Rothfuss, A., Sale, K., Young, M. M., Yang, C. L., Pancerella, C. M., and Fabris, D. (2008) The collaboratory for MS3D: A new cyberinfrastructure for the structural elucidation of biological macromolecules and their assemblies using mass spectrometry-based approaches. *J. Proteome Res. 7*, 4848−4857.
(48) Shaw, P. M., Hosea, N. A., Thompson, D. V., Lenius, J. M., and Guengerich, F. P. (1997) Reconstitution premixes for assays using purified recombinant human cytochrome P450, NADPH-cytochrome P450 reductase, and cytochrome b5. *Arch. Biochem. Biophys. 348*, 107−115.
(49) Kaspera, R., Naraharisetti, S. B., Evangelista, E. A., Marciante, K. D., Psaty, B. M., and Totah, R. A. (2011) Drug metabolism by CYP2C8.3 is determined by substrate dependent interactions with cytochrome P450 reductase and cytochrome b5. *Biochem. Pharmacol. 82*, 681−691.

(50) Clarke, T. A., Im, S. C., Bidwai, A., and Waskell, L. (2004) The role of the length and sequence of the linker domain of cytochrome b5 in stimulating cytochrome P450 2B4 catalysis. *J. Biol. Chem. 279*, 36809−36818.
(51) Farooq, Y., and Roberts, G. C. (2010) Kinetics of electron transfer between NADPH-cytochrome P450 reductase and cytochrome P450 3A4. *Biochem. J. 432*, 485−493.
(52) Roberts, A. G., Campbell, A. P., and Atkins, W. M. (2005) The thermodynamic landscape of testosterone binding to cytochrome P450 3A4: Ligand binding and spin state equilibria. *Biochemistry 44*, 1353−1366.
(53) Yano, J. K., Wester, M. R., Schoch, G. A., Griffin, K. J., Stout, C. D., and Johnson, E. F. (2004) The structure of human microsomal cytochrome P450 3A4 determined by X-ray crystallography to 2.05-A resolution. *J. Biol. Chem. 279*, 38091−38094.
(54) Cunane, L. M., Chen, Z. W., Durley, R. C., and Mathews, F. S. (1996) X-ray structure of the cupredoxin amicyanin, from *Paracoccus denitrificans*, refined at 1.31 Å resolution. *Acta Crystallogr. D52*, 676−686.
(55) Van Der Spoel, D., Lindahl, E., Hess, B., Groenhof, G., Mark, A. E., and Berendsen, H. J. (2005) GROMACS: fast, flexible, and free. *J. Comput. Chem. 26*, 1701−1718.
(56) Berendsen, H. J. C., Van Der Spoel, D., and Drunen, R. V. (1995) Gromacs: A message-passing parallel molecular dynamics implementation. *Comput. Phys. Commun. 91*, 43−56.
(57) Lindahl, E., Hess, B., and Van Der Spoel, D. (2001) GROMACS 3.0: a package for molecular simulation and trajectory analysis. *J. Mol. Model.*, 306−317.
(58) Pettersen, E. F., Goddard, T. D., Huang, C. C., Couch, G. S., Greenblatt, D. M., Meng, E. C., and Ferrin, T. E. (2004) UCSF Chimera: A visualization system for exploratory research and analysis. *J. Comput. Chem. 25*, 1605−1612.
(59) Pierce, B. G., Hourai, Y., and Weng, Z. (2011) Accelerating protein docking in ZDOCK using an advanced 3D convolution library. *PloS One 6*, e24657.
(60) Ohta, Y., Kawato, S., Tagashira, H., Takemori, S., and Kominami, S. (1992) Dynamic structures of adrenocortical cytochrome P-450 in proteoliposomes and microsomes: Protein rotation study. *Biochemistry 31*, 12680−12687.
(61) Durley, R. C., and Mathews, F. S. (1996) Refinement and structural analysis of bovine cytochrome b5 at 1.5 Å resolution. *Acta Crystallogr. D52*, 65−76.
(62) Sirim, D., Widmann, M., Wagner, F., and Pleiss, J. (2010) Prediction and analysis of the modular structure of cytochrome P450 monooxygenases. *BMC Struct. Biol. 10*, 34.
(63) Im, S. C., and Waskell, L. (2011) The interaction of microsomal cytochrome P450 2B4 with its redox partners, cytochrome P450 reductase and cytochrome b_5. *Arch. Biochem. Biophys. 507*, 144−153.
(64) Hendrychova, T., Anzenbacherova, E., Hudecek, J., Skopalik, J., Lange, R., Hildebrandt, P., Otyepka, M., and Anzenbacher, P. (2011) Flexibility of human cytochrome P450 enzymes: Molecular dynamics and spectroscopy reveal important function-related variations. *Biochim. Biophys. Acta 1814*, 58−68.
(65) Hendrychova, T., Berka, K., Navratilova, V., Anzenbacher, P., and Otyepka, M. (2012) Dynamics and hydration of the active sites of mammalian cytochromes p450 probed by molecular dynamics simulations. *Curr. Drug Metab. 13*, 177−189.
(66) Noble, M. A., Girvan, H. M., Smith, S. J., Smith, W. E., Murataliev, M., Guzov, V. M., Feyereisen, R., and Munro, A. W. (2007) Analysis of the interactions of cytochrome b_5 with flavocytochrome P450 BM3 and its domains. *Drug. Metab. Rev. 39*, 599−617.
(67) Guryev, O. L., Gilep, A. A., Usanov, S. A., and Estabrook, R. W. (2001) Interaction of apo-cytochrome b5 with cytochromes P4503A4 and P45017A: Relevance of heme transfer reactions. *Biochemistry 40*, 5018−5031.
(68) Zhang, H., Hamdane, D., Im, S. C., and Waskell, L. (2008) Cytochrome b5 inhibits electron transfer from NADPH-cytochrome P450 reductase to ferric cytochrome P450 2B4. *J. Biol. Chem. 283*, 5217−5225.
(69) Zhang, H., Myshkin, E., and Waskell, L. (2005) Role of cytochrome b5 in catalysis by cytochrome P450 2B4. *Biochem. Biophys. Res. Commun. 338*, 499−506.
(70) Wen, B., Lampe, J. N., Roberts, A. G., Atkins, W. M., David Rodrigues, A., and Nelson, S. D. (2006) Cysteine 98 in CYP3A4 contributes to conformational integrity required for P450 interaction with CYP reductase. *Arch. Biochem. Biophys. 454*, 42−54.
(71) Zhang, H., Im, S. C., and Waskell, L. (2007) Cytochrome b5 increases the rate of product formation by cytochrome P450 2B4 and competes with cytochrome P450 reductase for a binding site on cytochrome P450 2B4. *J. Biol. Chem. 282*, 29766−29776.
(72) Roussel, F. K. K., and Halpert, J. R. (2000) The importance of SRS-1 residues in catalytic specificity of human cytochrome P450 3A4. *Arch. Biochem. Biophys. 374*, 269−278.
(73) Wen, B., Doneanu, C. E., Gartner, C. A., Roberts, A. G., Atkins, W. M., and Nelson, S. D. (2005) Fluorescent photoaffinity labeling of cytochrome P450 3A4 by lapachenole: identification of modification sites by mass spectrometry. *Biochemistry 44*, 1833−1845.
(74) Cojocaru, V., Winn, P. J., and Wade, R. C. (2007) The ins and outs of cytochrome P450s. *Biochim. Biophys. Acta 1770*, 390−401.
(75) Rui, L., Pochapsky, S. S., and Pochapsky, T. C. (2006) Comparison of the complexes formed by cytochrome P450cam with cytochrome b5 and putidaredoxin, two effectors of camphor hydroxylase activity. *Biochemistry 45*, 3887−3897.
(76) Berka, K., Hendrychova, T., Anzenbacher, P., and Otyepka, M. (2011) Membrane position of ibuprofen agrees with suggested access path entrance to cytochrome P450 2C9 active site. *J. Phys. Chem. A 115*, 11248−11255.
(77) Banci, L., Bertini, I., Rosato, A., and Scacchieri, S. (2000) Solution structure of oxidized microsomal rabbit cytochrome b5. Factors determining the heterogeneous binding of the heme. *Eur. J. Biochem. 267*, 755−766.